

> REPLACE THIS LINE WITH YOUR MANUSCRIPT ID NUMBER (DOUBLE-CLICK HERE TO EDIT) <

An adaptive weighting strategy for multi-sensor integrated navigation in urban areas

Rui Sun, *Member, IEEE*, Yeying Dai, Qi Cheng

Abstract—Integration of global navigation satellite systems (GNSS) with other sensors, such as inertial measurement units (IMU) and visual sensors, has been widely used to improve the positioning accuracy and availability of the vehicles for the Internet of Things (IoT) applications in smart cities. The traditional Extended Kalman Filter (EKF)-based fusion scheme, with the assumption of fixed measurements of different sensors and inaccurate GNSS quality assessment, is vulnerable to Non-line-of-Sight (NLOS) and multipath contaminated GNSS, as well as low-quality vision measurement. In order to tackle this issue, we have proposed an adaptive weighting strategy for GNSS/IMU/Vision integration. On the basis of dual-check GNSS assessment, we adjust the weights of the vision and GNSS measurements adaptively based on the chi-square test statistic. The field tests have demonstrated that the proposed algorithm achieves horizontal positioning root mean square errors (RMSEs) of 11.92 m and 3.61 m in deep and mild urban environments. The accuracy has improvements of 78.57% and 43.9% over traditional EKF-based GNSS/IMU fusion, and 21.53% and 23.49% over compared EKF-based GNSS/IMU/Vision fusion, respectively.

Index Terms— Adaptive Kalman filter, Integrated navigation, Vision.

I. INTRODUCTION

In the Internet of Things (IoT) technology, each object needs to know its own and others' statuses and then exchanges their information over the Internet. Accurate and reliable Positioning, Navigation and Timing (PNT) information is essential for each object in IoT networks. GNSS and its multi-sensor navigation system can provide PNT information and play an increasingly important role in IoT applications such as Internet of Vehicle (IoV) and autonomous driving [1]. GNSS signals are easily contaminated by multipath and NLOS reception in built environments, leading to the excessive positioning errors [2]. One solution to this problem is integrating IMU with GNSS,

This work was supported in part by the sponsorship of the National Natural Science Foundation of China (Grant No. 42222401, 41974033, 42174025), the Natural Science Foundation of Jiangsu Province (Grant No. BK20211569), Fundamental Research Funds for the Central Universities (Grant No. xcjh20220722) and the University Grants Committee of Hong Kong under the scheme Research Impact Fund (Grant No. R5009-21), Research Institute of Land and System, Hong Kong Polytechnic University. (*Corresponding author: Qi. Cheng*)

R. Sun and Y. Dai are with the College of Civil Aviation, Nanjing University of Aeronautics and Astronautics, Nanjing 210016, China (e-mail: rui.sun@nuaa.edu.cn; yeying.dai@nuaa.edu.cn).

Qi Cheng is with the Department of Land Surveying and Geo-Information, the Hong Kong Polytechnic University, Hong Kong, China (e-mail: qi001.cheng@connect.polyu.hk).

and this has been shown to improve the positioning accuracy and reliability in urban areas [3][4]. But IMU errors accumulate in the absence of GNSS [5]. Thus, the persistent contaminated GNSS signals, or even long GNSS outages in urban areas will still result in rapid reductions in the performance of the integrated navigation [6]. Besides IMU, other sensors, including lidars, cameras and odometers, have been used to limit the reduction in performance [7]. The complementarity and economic feasibility of visual sensors has meant that these have been extensively adopted in such integrated navigation systems [8]. In complex urban environments, visual sensors obtain more feature points, such as foliage, buildings, or other complex objects [9], helping to improve the quality of the vision measurement. While in open areas, the lack of feature points in the images will degrade the quality of the vision measurement, but the GNSS signals are not shadowed.

Multi-sensor fusion algorithms are mainly based on filter or graph optimization [10]. According to whether the feature information of the image is added into the state vector, they are divided into loosely coupled and tightly coupled. MSCKF is a filter-based and tightly-coupled VIO framework with a measurement model of the geometric constraints observed from multiple cameras poses [11]. VINS is a very advanced monocular VIO tightly coupled algorithm based on nonlinear optimization and sliding windows [12]. Its loop detection can correct accumulated drift. The final drift with loop closure is (-0.032, 0.09, -0.07) m in xyz-axis. However, the loop closure is post-processing, and not applicable to real-time vehicle navigation. GVINS further realizes GNSS and VIO tightly coupled based on factor graph optimization, achieving accurate and continuous positioning in complex environment with a positioning accuracy of 4.508 m in urban driving experiment [13]. The theory and model are more complex, and the computation load is relatively large. In the filter based fusion algorithms, EKF is the most common fusion framework. Federated filter and particle filter are also used as the architecture for fusion [14]. However, these algorithms only change the filter type, and lack the research of adaptive strategy for sensor access and fusion. In [15], an EKF-based integrated camera/IMU/GNSS system is developed, using a GNSS differential technique to resolve the scale ambiguity problem of a monocular camera. Similarly, IMU data were denoised before integration with an 3D positioning accuracy improvement of 58% over traditional GNSS/INS integration [16]. However, they only focus on the performance of a single sensor.

> REPLACE THIS LINE WITH YOUR MANUSCRIPT ID NUMBER (DOUBLE-CLICK HERE TO EDIT) <

These algorithms perform quite differently in different scenarios due to lack of adaptivity. In fact, adaptive switch of the algorithm and the sensor data quality assessment is the basis of the adaptivity in the changeable urban environment. GNSS signals were divided into different modes according to Dilution of Precision (DOP), and switch strategy depending on different modes [17][18]. The algorithm improves positioning accuracy by 27.4% in [18]. The accuracy of the algorithm in [17] with KITTI dataset in a relatively open environment can reach an accuracy of less than 1 m, but its performance in complex urban environments has not been verified. Although their experimental results showed improvements in positioning accuracy, only DOP-based GNSS modes determination method still lacks reliability. In [19], meanwhile, the Kalman Filter residuals are calculated to determine if the GNSS measurement should be used in the positioning calculation. This system is not robust enough because the reliability of this judgment cannot be absolutely guaranteed. [20] established a robust Kalman Filtering based GNSS/IMU/VO integrated navigation, using chi-square statistic to adjust the measurement noise covariance. This method, is not always significantly effective due to the limited ability to adjust the measurement noise covariance and the fact that it is only sensitive to abrupt errors.

In conclusion, current research for GNSS/IMU/Vision integration still has some issues to be solved. In most of the research, the quality assessment for GNSS is not accurate and reliable. In addition, the current fusion strategy is always based on the fixed fusion mode, which has the degraded performance on the complex changing environments. In this paper, we propose a GNSS quality assessment model with an adaptive weighting strategy for GNSS/IMU/Vision integrated navigation system. The main contributions of this paper are as follows:

- A Geometrical Dilution of Precision (GDOP)-based GNSS measurement assessment model and a further chi-square test recheck model are proposed to assess the quality of GNSS measurement to support subsequent integrated navigation. Both GDOP value and chi-square test are used to ensure the accuracy of the assessment.
- We propose a chi-square test statistic based respective scale factor model to obtain an adaptive weighting strategy for the GNSS, IMU and vision measurements in the fusion process. The proposed fusion model is able to improve the adaptability.

II. PROPOSED INTEGRATION ARCHITECTURE

The proposed fusion algorithm based on the loosely coupled EKF scheme is shown in Fig. 1. This algorithm includes three steps. In step 1, based on the satellite number and GDOP value, GNSS measurement is determined into three statuses: unavailable, acceptable and to be further rechecked. Meanwhile, the data from the IMU and camera are processed to output the position, velocity, and attitude. In step 2, according to the result of the GNSS status assessed in step 1, if

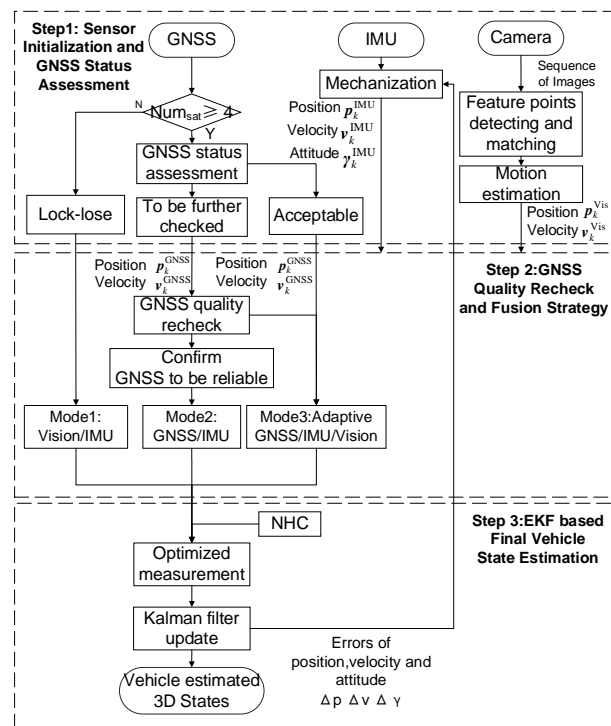


Fig.1. Algorithm Scheme

the GNSS measurement is unavailable, the vision measurement will be fused directly with IMU. If the GNSS measurement needs to be further rechecked, and then passes the GNSS quality recheck in step2, the GNSS measurement is considered as reliable and will be used directly as measurement to be fused with IMU. If the GNSS measurement does not pass the quality recheck, it is considered as acceptable. The adaptive weighting strategy will be used to fuse GNSS/IMU/Vision. In step 3, Non-Holonomic Constraint (NHC) is applied into the updating stage of EKF to obtain the state estimation of the vehicle, including position, velocity and attitude.

A. Coordinate frames

In this paper, the angular rate and specific force are generated in the body frame, whose origin is the center of the IMU, and the x, y, z axes are in the direction of front, right, down of the vehicle. The two coordinate frames for GNSS are the geodetic coordinate frame, including Latitude, Longitude, Height (BLH) frame and Earth Center Earth Fixed (ECEF) frame. The vision data is expressed in the camera frame originally, whose origin is the optical center and whose three axes are right, down, front of the camera. The data from all the sensors for further fusion are converted into the navigation frame (n -frame): North, East, Down (NED) frame.

B. GNSS mode identification and data processing

1) GDOP

In step 1, our integration framework starts with assessing the status of GNSS measurement so as to be able to choose among different specific strategies. If there are fewer than four satellites, GNSS does not have positioning and velocity

> REPLACE THIS LINE WITH YOUR MANUSCRIPT ID NUMBER (DOUBLE-CLICK HERE TO EDIT) <

solution, so we deem GNSS as unavailable. If there are more than four satellites, a GDOP based assessment is proposed with one threshold value because GDOP can reflect the geometric configuration of the satellite constellations which affects the accuracy of GNSS positioning [21]. If the GDOP value is small, the positioning accuracy is likely to be high, but if the GDOP value is large, the positioning quality is always poor. Following [22], GDOP depends on the design matrix. It can be defined as:

$$GDOP = \sqrt{\text{trace}[(A^T A)^{-1}]} \quad (1)$$

where, A can be used for indicating the receiver-satellite geometry, which is given by [23]:

$$A = \begin{pmatrix} \frac{\mathbf{p}_s^1 - \mathbf{p}_r}{\|\mathbf{p}_s^1 - \mathbf{p}_r\|} & 1 \\ \frac{\mathbf{p}_s^i - \mathbf{p}_r}{\|\mathbf{p}_s^i - \mathbf{p}_r\|} & 1 \\ \dots & \dots \\ \frac{\mathbf{p}_s^N - \mathbf{p}_r}{\|\mathbf{p}_s^N - \mathbf{p}_r\|} & 1 \end{pmatrix}_{N \times 4} \quad (2)$$

where, \mathbf{p}_s^i is the position of satellite i ; \mathbf{p}_r is the receiver approximate position in ECEF coordinate frame; N is the number of visible satellites at current epoch.

We set a threshold thr_1 to compare with the GDOP at each epoch to assess the GNSS quality. If the GDOP value is smaller than thr_1 , we still cannot ensure its quality because a small GDOP value cannot guarantee a small positioning error. Therefore, the GNSS data needs to be further rechecked in step 2 to confirm whether it is accurate enough for GNSS/IMU fusion. When the GDOP value exceeds thr_1 , due to the poor satellite geometry, GNSS is assessed as acceptable for further processing. The threshold is an empirical value.

$$\begin{cases} GDOP \geq thr_1 & \text{acceptable} \\ GDOP < thr_1 & \text{to be further rechecked} \end{cases} \quad (3)$$

2) GNSS position and velocity solution

To calculate the position and velocity of GNSS measurement for further fusion, this paper chooses pseudorange single point positioning and Doppler velocimetry methods. The pseudorange observations between the satellites and the receiver can be obtained by multiplying the propagation time of the GNSS signal from the satellite to the receiver by the speed of light. The pseudorange observations ρ can be expressed as [24]:

$$\rho = L + c(\delta t_s^i - \delta t_r) + V_{ion} + V_{trop} + \varepsilon \quad (4)$$

where, L represents the geometric range between the observed satellite i and the receiver; c is the speed of light in a vacuum; δt_s^i and δt_r are the clock error of satellite i and the receiver, respectively; V_{ion} and V_{trop} are, respectively, the delays caused by the ionosphere and troposphere; ε

represents the other errors, mainly caused by NLOS/multipath signals.

$$L = \sqrt{(x_s^i - x_r)^2 + (y_s^i - y_r)^2 + (z_s^i - z_r)^2} \quad (5)$$

where, (x_r, y_r, z_r) and (x_s^i, y_s^i, z_s^i) are the coordinates of the receiver and the satellite i in an ECEF coordinate system. After correcting ionospheric and tropospheric delays, with Klobuchar model and Saastamoinen model respectively, and obtaining satellite clock offset corrections and satellite position from broadcast ephemeris, least square method is used for positioning. Ultimately, the position of the receiver $\mathbf{p}_k^{\text{GNSS}}$ and clock error of the receiver t_r is solved [25].

In raw Doppler velocimetry method, the measurement model is:

$$\lambda D = \dot{\rho} + c(\delta t_s^i - \delta t_r) + \dot{V}_{ion} + \dot{V}_{trop} + \dot{\varepsilon} \quad (6)$$

$$\dot{\rho} = \frac{\mathbf{p}_r - \mathbf{p}_s^i}{\rho} \cdot (\mathbf{v}_r - \mathbf{v}_s^i) \quad (7)$$

where, λ is the wavelength; D is the Doppler shift; $\dot{\rho}$ is the pseudorange rate; δt_s^i and δt_r are the satellite clock drift and receiver clock drift, respectively; \dot{V}_{ion} and \dot{V}_{trop} are the rates of change in the ionospheric and tropospheric delays, respectively; $\dot{\varepsilon}$ is the rate of change in the other errors; \mathbf{v}_r and \mathbf{v}_s^i are the velocity of the receiver and satellite i , respectively.

Let $u = (\mathbf{p}_r - \mathbf{p}_s^i) / \rho$, the observation equation as:

$$[u \ 1] \cdot \begin{bmatrix} \mathbf{v}_r \\ \delta t_r \end{bmatrix} = u \cdot \mathbf{v}_s^i + \lambda D + \dot{\varepsilon} \quad (8)$$

Then calculate the receiver velocity \mathbf{v}_r in the ECEF frame through least squares method when observe more than four satellites.

3) Vision data processing

We use Zhang Zhengyou calibration method to calibrate our camera. We made a calibration target to measure the parameters of the stereo camera shown in Fig. 2. Each black and white square grid has a side length of 35 mm. We take a group of photos from different directions, totally 25 pictures for each camera. Through the one-to-one correspondence between multiple actual points in world coordinate and feature points on the picture in pixel coordinates, the correspondence between world coordinates and pixel coordinates can be obtained. Then, the intrinsic matrix and distortion parameters of each camera and the rotation and translation of the right camera to the left camera can be obtained.

For each camera frame, corner features are detected, and previous frames are tracked via KLT optical flow. The current frame is tracked based on the previous frame. For the stereo camera, the tracker also matches the features of the left and right images. The stereo images information of key frames is recorded in a sliding window with size of 10 frames [13]. If the average parallax of the new image exceeds the threshold, this frame will be added into the slide window as a key frame.

> REPLACE THIS LINE WITH YOUR MANUSCRIPT ID NUMBER (DOUBLE-CLICK HERE TO EDIT) <

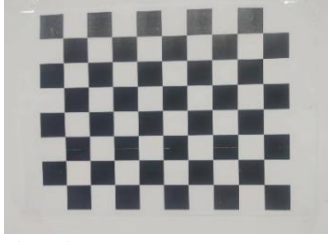


Fig. 2. Camera calibration target

Perspective-n-point (PnP) of 3D-2D is used for motion estimation. The rotation and translation are calculated based on minimize the reprojection error using least square method [26]. After solving the rotation and translation between two consecutive epochs, the rotation and translation with respect to the last epoch can be obtained. To tackle with the accumulated error of vision, we use the position of the integrated navigation result at the last epoch, and the velocity of vision at current epoch to calculate the position as vision position measurement.

C. GNSS quality recheck and fusion strategy

The navigation information from GNSS, IMU and vision is input into an adaptive EKF to obtain the state estimation. The loosely coupled system involves the position, velocity, and attitude of the vehicle, the three-axis bias of the accelerometer and the gyroscope, and the errors of the scale factor, modelled as a first-order Gauss-Markov process [27]. The 21-dimensional state vector built on the IMU estimation errors is described in (9):

$$\mathbf{X}_k = [\delta \mathbf{p}^n \ \delta \mathbf{v}^n \ \delta \gamma^n \ \mathbf{b}_g \ \mathbf{b}_a \ s_g \ s_a]^T \quad (9)$$

where, $\delta \mathbf{p}^n$, $\delta \mathbf{v}^n$, and $\delta \gamma^n$ represent the three-dimensional position, velocity and attitude error vectors in the navigation frame; \mathbf{b}_g and \mathbf{b}_a , respectively, represent the three-axis bias error vectors of the gyroscope and accelerometer in the body frame. s_g and s_a , respectively, represent the three-axis scale factor error vector of the gyroscope and accelerometer in the body frame.

Considering the high sampling rate of inertial navigation, the time interval Δt is very small. Therefore, the discretized Kalman filter is used in integrated navigation. For the linear discrete-time stochastic system, the error state transition equation is [28]:

$$\mathbf{X}_{k+1} = \Phi_{k+1,k} \mathbf{X}_k + \mathbf{W}_k \quad (10)$$

$$\mathbf{W}_k \sim N(0, \mathbf{Q}_k) \quad (11)$$

$\Phi_{k+1,k}$ can be approximated as:

$$\Phi_{k+1,k} = \exp\{\mathbf{F} \Delta t\} = \mathbf{I} + \mathbf{F} \Delta t \quad (12)$$

$$\Delta t = t_{k+1} - t_k \quad (13)$$

where, \mathbf{X}_{k+1} and \mathbf{X}_k are state vectors at $k+1$ and k epochs, respectively; $\Phi_{k+1,k}$ is the state transition matrix from k to $k+1$, set based on the error propagation of the IMU, derived from the IMU mechanization; \mathbf{F} is the dynamic matrix; \mathbf{W}_k is the system noise, and \mathbf{Q}_k is the system noise covariance matrix [29].

The measurement equation is as follows:

$$\mathbf{Z}_k = \mathbf{H}_k \mathbf{X}_k + \boldsymbol{\eta}_k \quad (14)$$

$$\boldsymbol{\eta}_k \sim N(0, \mathbf{R}_k) \quad (15)$$

where, \mathbf{Z}_k is the measurement vector; \mathbf{H}_k is the measurement matrix, composed of units 1 and 0, where 1 corresponds to the mapping of the position error and velocity error from the first six units in the state vector to the measurement vector; $\boldsymbol{\eta}_k$ is the measurement noise; \mathbf{R}_k is the measurement noise covariance matrix.

During the process of Kalman filter, the first phase is prediction. The IMU errors are predicted according to the error propagation principle of IMU sensors, which is later fed back to correct the parameters in IMU mechanization.

Prediction phase [30]:

$$\bar{\mathbf{X}}_{k+1} = \Phi_{k+1,k} \hat{\mathbf{X}}_k \quad (16)$$

$$\bar{\mathbf{P}}_{k+1} = \Phi_{k+1,k} \hat{\mathbf{P}}_k + \mathbf{Q}_k \quad (17)$$

where, \mathbf{P}_k is the state covariance matrix; The hats ' - ' and ' ^ ' indicate predicted and updated vector, respectively.

The measurement update scheme according to the three determined modes is introduced next. If the status of GNSS data is identified as unavailable, the fusion strategy is mode1, which is Vision/IMU integration. The data from vision is input into the measurement vector. The measurement vector has six dimensions composed of IMU and vision position and velocity:

$$\mathbf{Z}_k^{\text{M1}} = \begin{bmatrix} \mathbf{p}_k^{\text{IMU}} - \mathbf{p}_k^{\text{Vis}} \\ \mathbf{v}_k^{\text{IMU}} - \mathbf{v}_k^{\text{Vis}} \end{bmatrix} \quad (18)$$

where, \mathbf{Z}_k^{M1} is the measurement vector when GNSS is in mode 1 at epoch k ; $\mathbf{p}_k^{\text{IMU}}$ and $\mathbf{p}_k^{\text{Vis}}$ are position vectors of IMU and vision, respectively, at epoch k ; $\mathbf{v}_k^{\text{IMU}}$ and $\mathbf{v}_k^{\text{Vis}}$ are velocity vectors of IMU and vision, respectively, at epoch k .

If the GNSS data is identified to be further rechecked, we propose a GNSS recheck model to confirm whether GNSS measurement can be assessed as accurate. Firstly, we construct the measurement vector with six dimensions composed of the position and velocity of IMU and GNSS:

$$\mathbf{Z}_k^{\text{GNSS}} = \begin{bmatrix} \mathbf{p}_k^{\text{IMU}} - \mathbf{p}_k^{\text{GNSS}} \\ \mathbf{v}_k^{\text{IMU}} - \mathbf{v}_k^{\text{GNSS}} \end{bmatrix} \quad (19)$$

We use GNSS chi-square test here to perform the quality recheck. The innovation $\mathbf{r}_k^{\text{GNSS}}$ is defined as the difference between the measurement vector and the prediction of the measurement. It can be calculated as:

$$\mathbf{r}_k^{\text{GNSS}} = \mathbf{Z}_k^{\text{GNSS}} - \mathbf{H}_k \bar{\mathbf{X}}_k \quad (20)$$

In the case of optimal estimation by filtering, when the measurement is not disturbed by the faults, the innovation should be a white noise sequence with zero mean and standard Gaussian distribution, namely:

$$\mathbf{r}_k^{\text{GNSS}} \sim N(0, \mathbf{C}_k) \quad (21)$$

where, the corresponding covariance matrix \mathbf{C}_k is as follows:

> REPLACE THIS LINE WITH YOUR MANUSCRIPT ID NUMBER (DOUBLE-CLICK HERE TO EDIT) <

$$\mathbf{C}_k = E[\mathbf{r}_k^{\text{GNSS}^T} \cdot \mathbf{r}_k^{\text{GNSS}}] = \mathbf{H}_k \bar{\mathbf{P}}_k \mathbf{H}_k^T + \mathbf{R}_k \quad (22)$$

When there are abnormal faults in the measurement, the original properties of the innovation will be destroyed, resulting in the loss of its zero-mean characteristic and a certain offset in its probability distribution. The innovation will be affected by the faults, and the change will be reflected in the value of S_k^{GNSS} . Therefore, the faults can be detected by chi-square χ^2 test statistic. The innovation chi-square test statistic of GNSS is defined as [31]:

$$S_k^{\text{GNSS}} = (\mathbf{r}_k^{\text{GNSS}})^T \mathbf{C}_k^{-1} \mathbf{r}_k^{\text{GNSS}} \quad (23)$$

where, S_k^{GNSS} follows a chi-square distribution with d degrees of freedom, d is the dimension of the measurement. There are two binary hypotheses:

$$\begin{cases} \mathbf{H}_0: S_k^{\text{GNSS}} \sim \chi^2(d, 0) \\ \mathbf{H}_1: S_k^{\text{GNSS}} \sim \chi^2(d, \lambda), \lambda \neq 0 \end{cases} \quad (24)$$

where, \mathbf{H}_0 is the null hypothesis, indicating that the entire model has no fault; \mathbf{H}_1 is the alternative hypothesis, indicating that the entire model has fault; $\chi^2(d, 0)$ represents the central chi-square distribution with d degrees of freedom; λ is the decentralization parameter.

For a given significance level α , the rejection domain of the test is:

$$\text{RD} = \{S_k^{\text{GNSS}} \geq \chi_\alpha^2(d)\} \quad (25)$$

where, $\chi_\alpha^2(d)$ is the α quantile of a chi-square distribution with d degrees of freedom. Let the maximum allowable value be the threshold thr_2 , $thr_2 = \chi_\alpha^2(d)$. When S_k^{GNSS} exceeds the threshold thr_2 , we reject the \mathbf{H}_0 hypothesis and accept the \mathbf{H}_1 hypothesis. This indicates that the GNSS measurement still has some faults. Otherwise, we accept the \mathbf{H}_0 hypothesis. It is considered that the innovation maintains the original zero-mean characteristic, and the measurement is not disturbed by faults. Therefore, the GNSS data is reliable and fusion mode 2 is used. The threshold thr_2 is an empirical value.

$$\begin{cases} S_k^{\text{GNSS}} > thr_2 & \text{acceptable} \\ S_k^{\text{GNSS}} \leq thr_2 & \text{reliable} \end{cases} \quad (26)$$

As mentioned above, if GNSS data is rechecked as reliable, we use fusion mode 2, integrating GNSS and IMU directly. In this condition, the environment is more like open sky, GNSS is in high accuracy but less feature points can be obtained in vision. This limits the accuracy of vision. There, to avoid deteriorate the integrated solution, vision is not used here. When GNSS is not reliable, always in challenging environments, abundant feature points enable to use vision but can't ensure the vision accuracy. Therefore, we use vision to aid positioning when GNSS has faults and errors in mode3.

For fusion mode 2, after the calculation of the GNSS position and velocity, we can obtain the measurement vector

in mode 2:

$$\mathbf{Z}_k^{\text{M2}} = \mathbf{Z}_k^{\text{GNSS}} = \begin{bmatrix} \mathbf{p}_k^{\text{IMU}} - \mathbf{p}_k^{\text{GNSS}} \\ \mathbf{v}_k^{\text{IMU}} - \mathbf{v}_k^{\text{GNSS}} \end{bmatrix} \quad (27)$$

where, \mathbf{Z}_k^{M2} is the measurement vector when GNSS is in mode 2 at k epoch.

When GNSS data is rechecked as acceptable, we use fusion mode3 GNSS/IMU/Vision integration. A weighting strategy is proposed to fuse the position and velocity of GNSS and vision for the adaptive construction of the measurement vector:

$$\mathbf{Z}_k^{\text{M3}} = \begin{bmatrix} \mathbf{p}_k^{\text{IMU}} - \mathbf{p}_k^{\text{GNSS/Vis}} \\ \mathbf{v}_k^{\text{IMU}} - \mathbf{v}_k^{\text{GNSS/Vis}} \end{bmatrix} \quad (28)$$

where, \mathbf{Z}_k^{M3} is the measurement vector when GNSS is acceptable at k epoch, $\mathbf{p}_k^{\text{GNSS/Vis}}$ and $\mathbf{v}_k^{\text{GNSS/Vis}}$ are the weighted position and velocity from GNSS and vision measurements. The weights are calculated with the chi-square statistic as follows.

We put the GNSS and vision measurements into the measurement vector, like \mathbf{Z}_k^{M1} and \mathbf{Z}_k^{M2} , to calculate two innovations $\mathbf{r}_k^{\text{GNSS}}$ and $\mathbf{r}_k^{\text{Vis}}$ respectively. $\mathbf{r}_k^{\text{GNSS}}$ is calculated in (20) and $\mathbf{r}_k^{\text{Vis}}$ can be calculated as:

$$\mathbf{r}_k^{\text{Vis}} = \mathbf{Z}_k^{\text{M1}} - \mathbf{H}_k \bar{\mathbf{X}}_k \quad (29)$$

Considering that the possible errors in three-dimensional position and velocity are different, we cannot assign the same weights to each component of the measurement. We calculate separate statistic for each component of \mathbf{Z}_k^{M3} and take single-dimension weighting strategy.

$$S_k^{\text{GNSS}}(j) = (\mathbf{r}_k^{\text{GNSS}})^T(j) \mathbf{C}_k \mathbf{r}_k^{\text{GNSS}}(j) \quad (30)$$

$$S_k^{\text{Vis}}(j) = (\mathbf{r}_k^{\text{Vis}})^T(j) \mathbf{C}_k \mathbf{r}_k^{\text{Vis}}(j) \quad (31)$$

where, j represents the j -th component of six dimensional innovations, $j=1,2,\dots,6$; S_k^{GNSS} and S_k^{Vis} represent the test statistic of the GNSS and vision data at epoch k , respectively. They can evaluate the difference between the predicted data and the actual measurement data [32]. The larger its value, the smaller the corresponding weight should be. The weights for GNSS and vision are then calculated as follows:

$$\mathbf{w}_{\text{GNSS}}(j, j) = \frac{S_k^{\text{Vis}}(j)}{S_k^{\text{GNSS}}(j) + S_k^{\text{Vis}}(j)} \quad (32)$$

$$\mathbf{w}_{\text{Vis}}(j, j) = \frac{S_k^{\text{GNSS}}(j)}{S_k^{\text{GNSS}}(j) + S_k^{\text{Vis}}(j)} \quad (33)$$

where, \mathbf{w}_{GNSS} and \mathbf{w}_{Vis} are the weight matrices of GNSS and vision. The weighted position $\mathbf{p}_k^{\text{GNSS/Vis}}$ and velocity $\mathbf{v}_k^{\text{GNSS/Vis}}$ are calculated as:

$$\begin{bmatrix} \mathbf{p}_k^{\text{GNSS/Vis}} \\ \mathbf{v}_k^{\text{GNSS/Vis}} \end{bmatrix} = \mathbf{w}_{\text{GNSS}} \begin{bmatrix} \mathbf{p}_k^{\text{GNSS}} \\ \mathbf{v}_k^{\text{GNSS}} \end{bmatrix} + \mathbf{w}_{\text{Vis}} \begin{bmatrix} \mathbf{p}_k^{\text{Vis}} \\ \mathbf{v}_k^{\text{Vis}} \end{bmatrix} \quad (34)$$

The process of the adaptive weighting strategy and related

> REPLACE THIS LINE WITH YOUR MANUSCRIPT ID NUMBER (DOUBLE-CLICK HERE TO EDIT) <

TABLE I

PSEUDO-CODE OF THE ADAPTIVE WEIGHTING STRATEGY

Algorithm: Adaptive weighting strategy.

Input: $N, \mathbf{r}_k^{\text{Vis}}, \mathbf{r}_k^{\text{GNSS}}, GDOP$

Output: the measurement vector \mathbf{Z}_k

- 1: **if** $N < 4$
- 2: $\mathbf{Z}_k = \mathbf{Z}_k^{\text{M1}}$
- 3: **else if** $GDOP < thr_1$
- 4: **calculate** S_k^{GNSS} and S_k^{Vis} based on (30)(31)
- 5: **if** $S_k^{\text{GNSS}} < thr_2$
- 6: $\mathbf{Z}_k = \mathbf{Z}_k^{\text{M2}}$
- 7: **else calculate the weights**, $\mathbf{Z}_k = \mathbf{Z}_k^{\text{M3}}$
- 8: **end**
- 9: **end**
- 10: **end**

TABLE II

SENSOR PARAMETERS OF STIM-300

Accelerometer	Bias instability	0.05 mg
	Random walk noise	0.06 m/s/sqrt(hr)
Gyroscope	Bias instability	0.5 deg/hr
	Random walk noise	0.15 deg/sqrt(hr)

TABLE III

SENSOR PARAMETERS OF D455

Resolution	848×480 pixel
Sampling rate	30Hz
Baseline	95mm

TABLE IV

SENSOR PARAMETERS OF HG4930

Accelerometer	Bias instability	0.025 mg
	Random walk noise	0.03 m/s/sqrt(hr)
Gyroscope	Bias instability	0.25 deg/hr
	Random walk noise	0.04 deg/sqrt(hr)

III. RESULTS AND DISCUSSION

A. Experimental process

Two vehicle field tests were executed to evaluate the performance of the proposed algorithm in urban areas, in Nanjing, Jiangsu, China. The single frequency GNSS raw measurement data, including pseudorange as well as Doppler measurement, was collected at a sampling rate of 10 Hz using a BDStar Navigation C520-AT receiver with board card NovAtel OEM 7500. The IMU raw data was collected using a MEMS IMU, STIM-300, at a sampling rate of 125 Hz, including the measurement of specific force and angular rate. Its corresponding parameters are given in Table II. The vision data was collected from an Intel Real-sense D455 camera at a sampling rate of 30 Hz. The parameters are shown in Table III. The reference of the trajectory used in the experiment was determined by integration of a high grade HGuide N580inertial sensor with RTK GNSS integration by Inertial Explore software in the post-processing mode. It can achieve accuracy of cm level. The IMU of N580 is Honeywell HG4930. Its parameters are given in Table IV. N580 was connected to antenna 1, and BDStar Navigation C520-AT GNSS receiver was connected to antenna 2, both being ZYACF-S806 antennas of Zhejiang ZhongYu Communication Technology Co., Ltd. The equipment layout is shown in Fig. 3.

Test case 1 was single constellation using GPS and test case 2 was multi-constellation using BDS and GPS. Test case 1 was in a deep urban environment, depicted in Fig. 4. There are many tall buildings and viaducts in this environment, resulting in severe GNSS outages and multipath error. Test case2 was in a relatively mild urban environment with narrow alley and buildings as shown in Fig. 5. Fig. 6 and Fig. 7 shows the GDOP and number of satellites in test case 1 and case 2.

To verify the effectiveness and performance of the proposed GNSS/IMU/Vision algorithm, the proposed algorithm is compared with two other algorithms. The description of the candidate algorithms are as follows:

- 1) Traditional GNSS/IMU algorithm: The traditional EKF based GNSS/IMU loosely-coupled integration navigation.

navigation mode switching is illustrated in pseudo-code in Table I.

D. EKF-based Final Vehicle State Estimation

Considering the vehicle will not exhibit lateral sliding, nor will it move along the road surface in the vertical direction, the following NHC can be applied to vehicles to improve the state estimation accuracy. For the final velocity measurement for fusion obtained from three modes, the component in the right (y) and down (z) directions in the body frame are zero. The velocity measurements in different modes are:

$$\mathbf{v}_k = \begin{cases} \mathbf{v}_k^{\text{Vis}} & \text{Mode1} \\ \mathbf{v}_k^{\text{GNSS}} & \text{Mode2} \\ \mathbf{v}_k^{\text{GNSS/Vis}} & \text{Mode3} \end{cases} \quad (35)$$

$$\mathbf{v}_k^{\text{b}} = [\mathbf{v}_k^{\text{b-x}} \ 0 \ 0]^T \quad (36)$$

where, \mathbf{v}_k is the velocity in the NED frame, and where \mathbf{v}_k^{b} represents the velocity in the body frame, and $\mathbf{v}_k^{\text{b-x}}$ represents the velocity component of axis x in the body frame. We convert the velocity from the navigation coordinate frame to the body frame in order to implement NHC and then be reverted to the NED frame for Kalman filtering.

Then, the update phase only executes at the epochs having GNSS and vision observations and thus to correct the divergence of inertial navigation errors [33].

$$\mathbf{K}_{k+1} = \bar{\mathbf{P}}_{k+1} \mathbf{H}_{k+1}^T (\mathbf{H}_{k+1} \bar{\mathbf{P}}_{k+1} \mathbf{H}_{k+1}^T + \mathbf{R}_{k+1})^{-1} \quad (37)$$

$$\hat{\mathbf{X}}_{k+1} = \bar{\mathbf{X}}_{k+1} + \mathbf{K}_{k+1} (\mathbf{Z}_{k+1} - \mathbf{H}_{k+1} \bar{\mathbf{X}}_{k+1}) \quad (38)$$

$$\hat{\mathbf{P}}_{k+1} = (\mathbf{I} - \mathbf{K}_{k+1} \mathbf{H}_{k+1}) \bar{\mathbf{P}}_{k+1} \quad (39)$$

where, $\hat{\mathbf{X}}_{k+1}$ and $\hat{\mathbf{P}}_{k+1}$ represents the estimated state vector and covariance matrix at epoch $k+1$; \mathbf{I} is the identity matrix and \mathbf{K}_{k+1} is the gain matrix at epoch $k+1$. The positioning, velocity and attitude errors in the $\hat{\mathbf{X}}_{k+1}$ are the output at current epoch to correct IMU accumulated errors to obtain the estimated vehicle 3D states.

> REPLACE THIS LINE WITH YOUR MANUSCRIPT ID NUMBER (DOUBLE-CLICK HERE TO EDIT) <



Fig. 3. The vehicle for test with equipment



Fig. 4. Test case 1 environment



Fig. 5. Test case 2 environment

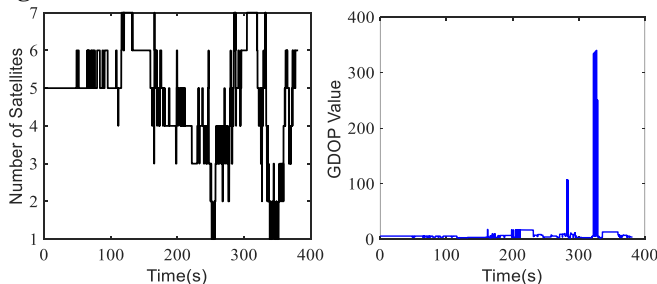


Fig. 6. Number of GPS satellites (left) and GDOP (right)

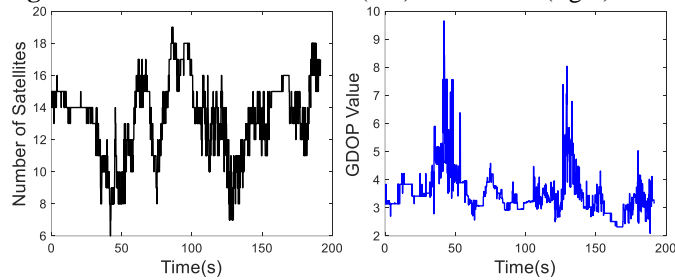


Fig. 7. Number of GNSS satellites (left) and GDOP (right)

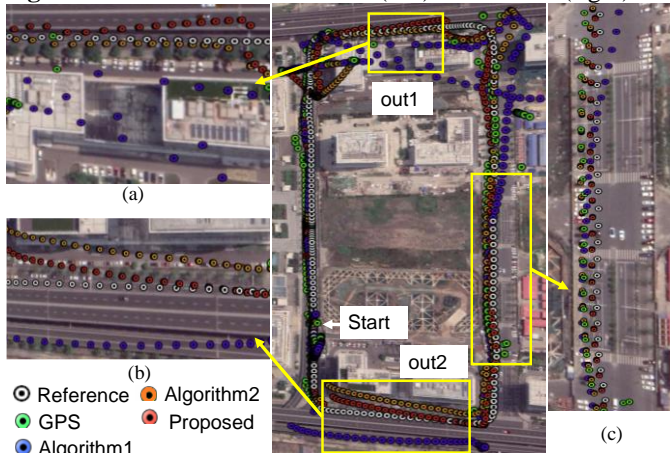


Fig. 8. Trajectories of the algorithms in the test case 1

- 2) GNSS/IMU/Vision algorithm: Like [17-18], this only uses the GDOP value, compared with $thr1$ to identify the GNSS status to choose GNSS or vision data as measurement to be integrated with IMU.
- 3) Proposed algorithm: Adaptive weighting strategy-based GNSS/IMU/Vision integrated navigation. In test case 1, $thr1 = 7$, $thr2 = 200$; In test case2, $thr1 = 4$, $thr2 = 50$;

B. Experimental results evaluation

In test case 1, the field test was executed in a typical dense urban environment, where the GPS signals were frequently blocked and had several outages. The navigation trajectories of three algorithms are shown in Fig. 8. In the part (a) and (b), due to the viaducts, GPS have no positioning solution or huge multipath error. Algorithm 1 has unacceptable errors for a long time, while in the red trajectory, our proposed algorithm effectively reduces the errors at these epochs because the vision measurement corrects the IMU accumulated error in the GPS outages and huge GPS positioning errors. Besides, in Fig.8(c), when the GPS signal is normal, the accuracy of the proposed algorithm is still higher than other two algorithms.

The performance comparison is shown in Table V in terms of RMSEs. The result shows that our proposed algorithm is superior to the other two algorithms. The RMSEs of the proposed algorithm in horizontal and 3D positioning are 11.92 m and 13.58 m, with 7.84 m, 8.97 m, and 6.51 m in the NED frame. It thus improves the accuracy by 78.57% and 77.23% over algorithm 1, 21.53% and 42.48% over algorithm2 in horizontal and 3D, respectively. Velocity of the proposed algorithm reaches the accuracy of 0.83 m/s and 0.87 m/s in the horizontal and 3D velocity respectively, with improvement of 78.33% and 77.86% over algorithm 1, 26.55% and 36.96% over algorithm 2. The roll and pitch of the proposed algorithm are 0.36 degree and 0.32 degree, having improvement of 55.56% and 51.52% over algorithm 1, and 16.28% and 3.03% over algorithm 2. The RMSE of heading is 2.14 degrees, slightly larger than roll and pitch, but still attains improvement 85.73% algorithm 1 and 38.51% over algorithm 2.

The comparison among the position, velocity and attitude errors of these three algorithms is shown in Fig. 9-11. The vehicle was stationary initially. In the stationary period, we can find that the results of algorithms 1 and 2 are very similar. This means that the quality of GPS measurement passes the assessment of algorithm 2, and vision is not used here. However, during this period, the accuracy of GPS positioning is frequently affected by multipath errors. These errors are mitigated by the proposed strategies in algorithm 3. In the dynamic test, in Fig. 9, the performance of the proposed algorithm also provides great improvements over the comparison methods. There are several outages during about 200~250s, 320~370s. In these two periods, only few epochs GPS can solve position and velocity. Nevertheless, there are huge errors at these epochs due to challenging environments. In algorithm 1, due to the lack of GPS measurement assessment, huge errors in velocity deteriorate the attitudes rapidly. While in algorithms 2 and 3, these bad GPS

> REPLACE THIS LINE WITH YOUR MANUSCRIPT ID NUMBER (DOUBLE-CLICK HERE TO EDIT) <

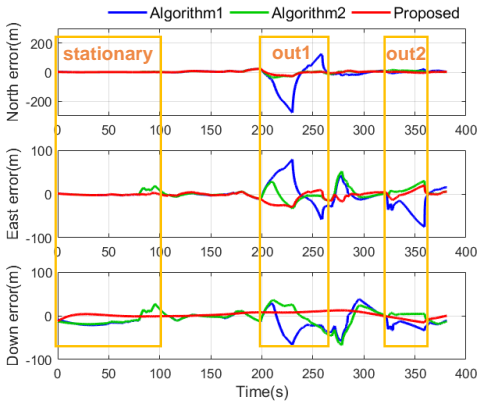


Fig. 9. Comparison of position error in test case 1

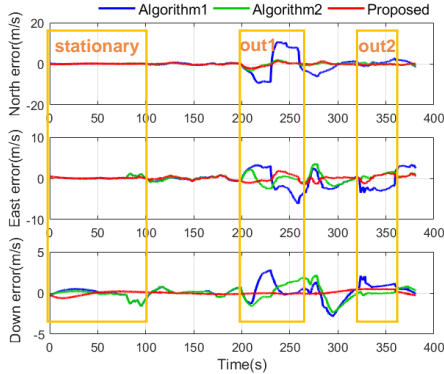


Fig. 10. Comparison of velocity error in test case 1

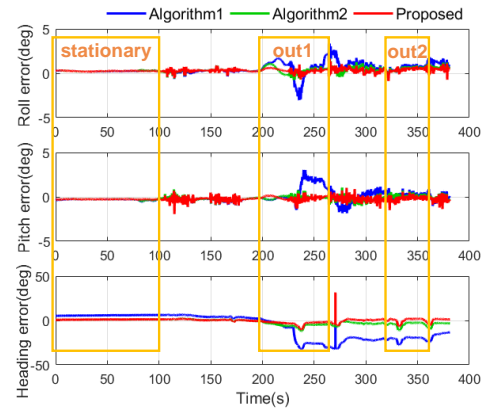


Fig. 11. Comparison of attitude error in test case 1

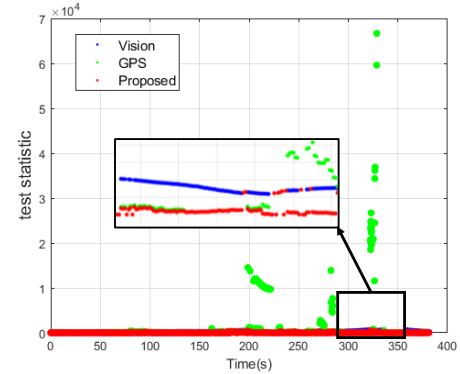


Fig. 12. Comparison of Chi-square statistics in test case 1

TABLE V

PERFORMANCE ANALYSIS OF THE THREE ALGORITHMS IN TEST CASE 1

RMSE		Algorithm1	Algorithm2	Proposed	Improvement over Algorithm1(%)	Improvement over Algorithm2(%)
Position (m)	North	50.81	10.06	7.84	84.57%	22.07%
	East	22.62	11.39	8.97	60.34%	21.25%
	Down	21.57	18.07	6.51	69.82%	63.97%
	Horizontal	55.62	15.19	11.92	78.57%	21.53%
	3D	59.65	23.61	13.58	77.23%	42.48%
Velocity (m)	North	3.37	0.68	0.58	82.79%	14.71%
	East	1.81	0.91	0.59	67.40%	35.16%
	Down	0.90	0.79	0.24	73.33%	69.62%
	Horizontal	3.83	1.13	0.83	78.33%	26.55%
	3D	3.93	1.38	0.87	77.86%	36.96%
Attitude (degree)	Roll	0.81	0.43	0.36	55.56%	16.28%
	Pitch	0.66	0.33	0.32	51.52%	3.03%
	Heading	15.00	3.48	2.14	85.73%	38.51%

measurements are excluded or weighted mostly, they can significantly and accurately bridge these outages using Vision or weighted measurements. The result of proposed algorithm is a little better than that of algorithm 2 due to more accurate assessment and flexible strategies. Besides these outages, the proposed algorithm still performs better than the other two algorithms. The accurate GPS status assessment can make better use of both vision data and GPS measurements. The proposed weighting strategy take both accuracy and robustness into account, fusing the two measurements according to their statistic. In Fig. 11, similar to the position error figure, attitude estimation can also be improved by the position and velocity correction.

To further investigate the effectiveness of the proposed algorithm, the chi-square statistic is shown in Fig. 12. We zoom in one part of the statistic at 300~350s. In the enlarged part, the chi-square test statistic of our proposed algorithm is

the smallest among the three sets of statistic. Specifically, some test statistic of proposed algorithm is equal to the vision statistic(blue) because at these epochs, GPS is unavailable and we only use vision as observation. This picture demonstrates that our algorithm can offer more accurate measurement compared with single GNSS or vision measurement.

In test case 2, a mild urban environment, the number of available satellites, including GPS and BDS, are much more than that in case 1. The trajectories are shown in Fig. 13. In the three enlarged parts, our proposed algorithm has the highest positioning accuracy when GNSS is disturbed by various degree multipath effect. In Table VI, the horizontal positioning accuracy of the proposed algorithm is 3.61m. with an improvement of 43.9% and 23.49% over algorithms 1 and 2, respectively. Our algorithm also has improvements in velocity and attitude.

> REPLACE THIS LINE WITH YOUR MANUSCRIPT ID NUMBER (DOUBLE-CLICK HERE TO EDIT) <

TABLE VI
PERFORMANCE ANALYSIS OF THE THREE ALGORITHMS IN TEST CASE 2

RMSE		Algorithm1	Algorithm2	Proposed	Improvement over Algorithm1(%)	Improvement over Algorithm2(%)
Position (m)	North	4.17	3.95	2.79	33.09%	29.37%
	East	4.88	2.58	2.29	53.07%	11.24%
	Down	9.48	8.91	4.44	53.16%	50.17%
	Horizontal	6.43	4.72	3.61	43.90%	23.49%
	3D	11.46	10.08	5.72	50.06%	43.25%
Velocity (m)	North	0.23	0.22	0.18	21.74%	18.18%
	East	0.31	0.17	0.15	51.61%	11.76%
	Down	0.40	0.38	0.16	60.0%	57.89%
	Horizontal	0.39	0.28	0.23	39.30%	15.73%
	3D	0.56	0.47	0.28	48.96%	39.74
Attitude (degree)	Roll	0.16	0.14	0.13	18.75%	7.14%
	Pitch	0.11	0.09	0.09	18.18%	0.00%
	Heading	2.53	2.59	2.49	1.58%	3.86%

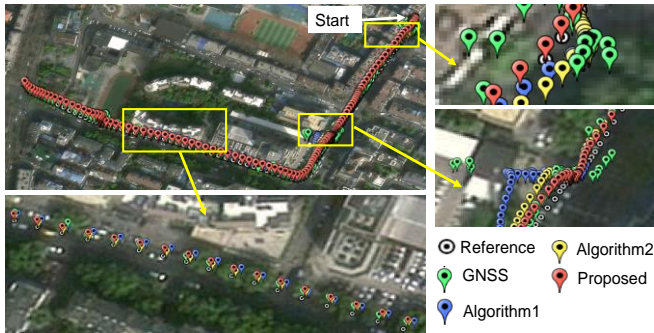


Fig. 13. Trajectories of the algorithms in test case 2

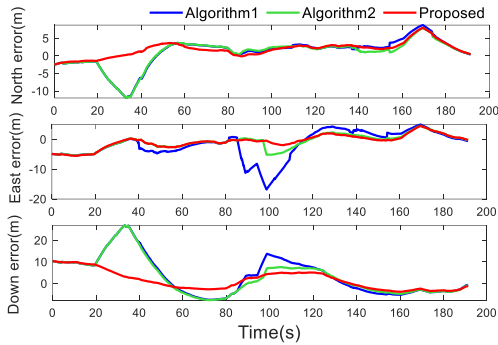


Fig. 14. Comparison of position error in the test case 2

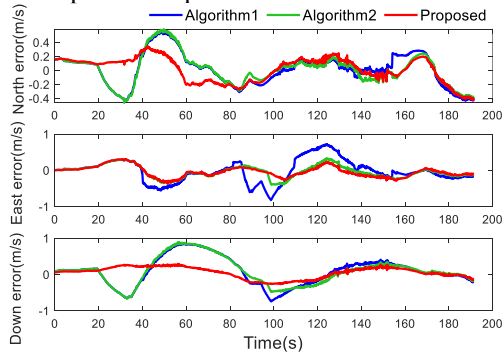


Fig. 15. Comparison of velocity error in test case 2

The comparison among the position, velocity and attitude error of these three algorithms is shown in Fig. 14-16. In regard to position and velocity accuracy, the proposed algorithm is the best one in the whole test. Although at some epochs, the attitude errors of the proposed algorithm get worse, on the whole, the accuracy of the proposed algorithm performs better than algorithm1 and 2.

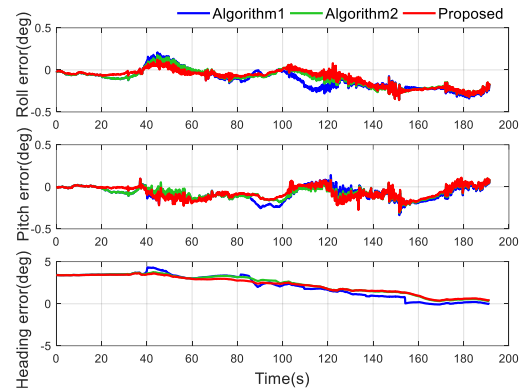


Fig. 16. Comparison of attitude error in the test case 2

IV. CONCLUSION

This paper has developed a GNSS status assessment model and an adaptive weighting strategy based Kalman filter algorithm for loosely coupled GNSS/IMU/Vision integration in urban areas. The result shows that the proposed algorithm can improve the performance of position, velocity and attitude estimation, achieving horizontal positioning RMSEs of 11.92m and 3.61m in deep and mild urban environments. The accuracy has an improvement of 78.57% and 43.9% over traditional EKF-based GNSS/IMU fusion, and 21.53% and 23.49% over compared EKF-based GNSS/IMU/Vision fusion, respectively. The proposed algorithm is suitable for vehicles with low-cost onboard GNSS, IMU and camera sensors for IoT applications. In the future, the algorithm performance could be further improved by modelling and correcting vision sensor error, as well as regional GNSS correction services.

REFERENCES

- [1] S. Li, S. Wang, Y. Zhou and Z. Shen, "Tightly coupled integration of GNSS, INS and LiDAR for vehicle navigation in urban environments," *IEEE Internet of Things Journal*, 2022.
- [2] R. Sun, Z. Zhang, Q. Cheng and W. Y. Ochieng, "Pseudorange error prediction for adaptive tightly coupled GNSS/IMU navigation in urban areas," *GPS Solutions*, vol.26, no.1, pp.1-13, Dec.2022.
- [3] Y. Mao, R. Sun, J. Wang, Q. Cheng, L. Kiong and W. Y. Ochieng, "New time-differenced carrier phase approach to GNSS/INS integration," *GNSS Solutions*, vol.26, no.4, pp.1-13, Aug.2022.
- [4] R. Sun, J. Wang, Q. Cheng, Y. Mao and W. Y. Ochieng, "A new IMU-aided multiple GNSS fault detection and exclusion algorithm for integrated navigation in urban environments," *GNSS Solutions*, vol.25, no.4, pp.1-17, Oct.2021.

> REPLACE THIS LINE WITH YOUR MANUSCRIPT ID NUMBER (DOUBLE-CLICK HERE TO EDIT) <

- [5] X. Li, H. Wang, S. Li, S. Feng, X. Wang and J. Liao, "GIL: a tightly coupled GNSS PPP/INS/LiDAR method for precise vehicle navigation," *Satell. Navig.*, vol.2, no.1, pp.1-17, Nov.2021.
- [6] R. Sun, G. Wang, Q. Cheng, L. Fu, K. Chiang, L. T. Hsu and W. Y. Ochieng, "Improving GNSS Code Phase Positioning Accuracy in Urban Environments Using Machine Learning," *IEEE Internet of Things Journal*, vol.8, no.8, pp.7065-7078, Apr.2021.
- [7] K. Chiang, G. Tsai, H. Chang, C. Joly and N. El-Sheimy, "Seamless navigation and mapping using an INS/GNSS/grid-based SLAM semi-tightly coupled integration scheme," *Information Fusion*, vol.50, pp.181-196, Oct.2019.
- [8] F. Liu, Y. B. Sarvrood and Y. Gao, "Implementation and analysis of tightly integrated INS/stereo VO for land vehicle navigation," *The Journal of Navigation*, vol.71, no.1, pp.83-99, Jan.2018.
- [9] X. Li, X. Wang, J. Liao, X. Li, S. Li and H. Lyu, "Semi-tightly coupled integration of multi-GNSS PPP and S-VINS for precise positioning in GNSS-challenged environments," *Satell. Navig.*, vol.2, no.1, pp.1-14, Jan.2021.
- [10] L. Zhao, X. Wang, J. Ding and W. Cao. "Review of nonlinear filtering algorithms for integrated navigation systems". *Chinese Journal of Inertial Technology*, vol.17(01), pp. 46-52+58,2009.
- [11] A I. Mourikis, S I. Roumeliotis. "A Multi-State Constraint Kalman Filter for Vision-aided Inertial Navigation," *ICRA*, 2007.
- [12] T. Qin, P. Li, S. Shen. "VINS-mono: A robust and versatile monocular visual-inertial state estimator," *IEEE Transactions on Robotics*, vol.34(4), pp.1004-1020, 2018.
- [13] S. Cao, X. Lu, S. Shen., "GVINS: Tightly coupled GNSS-visual-inertial fusion for smooth and consistent state estimation," *IEEE Transactions on Robotics*, 2022.
- [14] K. Shunsuke, G. Yanlei, L T. Hsu. "GNSS/INS/on-board camera integration for vehicle self-localization in urban canyon," *IEEE 18th International Conference on Intelligent Transportation Systems. IEEE*, pp.2533-2538, 2015.
- [15] T. Chu, N. Guo, S. Backén and D. Akos, "Monocular Camera/IMU/GNSS Integration for Ground Vehicle Navigation in Challenging GNSS Environments," *Sensors*, vol.12, no.3, pp.3162-3185, Mar.2021.
- [16] M. Nezhadshahbodaghi and M. R. Mosavi, "A loosely-coupled EMD-denoised stereo VO/INS/GPS integration system in GNSS-denied environments," *Measurement*, vol.183,2021.
- [17] Q. Su, Q. Tang, Y. Li and L. Liu, "GNSS-Aided Visual-Inertial Odometry with Failure Mode Recognition," *2021 4th International Conference on Intelligent Autonomous Systems (ICoIAS)*, pp.175-180, 2021.
- [18] D. H. Won, E. Lee, M. Heo, S. W. Lee, J. Lee, J. Kim and Y. J. Lee, "Selective integration of GNSS, vision sensor, and INS using weighted DOP under GNSS-challenged environments," *IEEE Transactions on Instrumentation and Measurement*, vol.63, no.9, pp.2288-2298,2014.
- [19] L. Xiong, R. Kang, J. Zhao, P. Zhang, M. Xu, R. Ju, C. Ye and T. Feng, "G-VIDO: A Vehicle Dynamics and Intermittent GNSS-Aided Visual-Inertial State Estimator for Autonomous Driving," *IEEE Transactions on Intelligent Transportation Systems*, vol. 23, no. 8, pp. 11845-11861, Aug. 2022.
- [20] B. Li, W. Chen, Y. Peng, D. Dong, Z. Wang, T. Xiao, C. Yu and M. Liu, "Robust Kalman Filtering Based on Chi-square Increment and Its Application," *Remote Sensing*, vol.12, no.4, pp.732, Feb.2020.
- [21] B. Liu, Y. Teng and Q. Huang, "GDOP minimum in multi-GNSS positioning," *Advances in Space Research*, vol.60, no.7, pp.1400-1403, Oct. 2017.
- [22] C. H. Wu, W. H. Su and Y. W. Ho, "A study on GNSS GDOP approximation using support-vector machines," *IEEE Transactions on Instrumentation and Measurement*, vol. 60, no. 1, pp. 137-145, Jan. 2011.
- [23] Y. Teng and J. Wang, Q. Huang, "Minimum of Geometric Dilution of Precision (GDOP) for five satellites with dual-GNSS constellations," *Advances in Space Research*, vol.56, no.2, Jul. 2015.
- [24] Q. Cheng, P. Chen, R. Sun, J. Wang, Y. Mao and W. Y. Ochieng, "A New Faulty GNSS Measurement Detection and Exclusion Algorithm for Urban Vehicle Positioning," *Remote Sensing*. vol.13, no.11, pp.2117, May.2021.
- [25] L. Ji, R. Sun, Q. Cheng, et al. "Evaluation of the performance of GNSS-based velocity estimation algorithms," *Satellite Navigation*, vol.3, no.1, pp.1-16, 2022.
- [26] Liu F, Sarvrood Y B, Gao Y. Implementation and analysis of tightly integrated INS/stereo VO for land vehicle navigation[J]. *The Journal of Navigation*, 2018, 71(1): 83-99.
- [27] M. Park, "Error analysis and stochastic modeling of MEMS based inertial sensors for land vehicle navigation applications," Canada, CALLARY, 2004.
- [28] Y. Le, X. He and R. Xiao, "MEMS IMU and GNSS/Beidou Integration Navigation System Using Interval Kalman Filter," *AMM*, vol. 568-570, pp.970-975, Jun.2014.
- [29] G. Wan, X. Yang, R. Cai, H. Li, Y. Zhou, H. Wang and S. Song "Robust and Precise Vehicle Localization Based on Multi-Sensor Fusion in Diverse City Scenes," 2018 IEEE International Conference on Robotics and Automation (ICRA), pp. 4670-4677, May.2018.
- [30] A. Vu, A. Ramanandan, A. Chen, J. A. Farrell and M. Barth, "Real-Time Computer Vision/DGNSS-Aided Inertial Navigation System for Lane-Level Vehicle Navigation," *IEEE Transactions on Intelligent Transportation Systems*, vol. 13, no. 2, pp. 899-913, June 2012.
- [31] G. Hu, W. Wang, Y. Zhong, B. Gao and C. Gu, "A new direct filtering approach to INS/GNSS integration," *Aerospace Science and Technology*, vol.77, pp.755-764, Jun.2018.
- [32] H. Xiong, R. Bian, Y. Li, Z. Du and Z. Mai, "Fault-Tolerant GNSS/SINS/DVL/CNS Integrated Navigation and Positioning Mechanism Based on Adaptive Information Sharing Factors," *IEEE Systems Journal*, vol. 14, no. 3, pp. 3744-3754, Sept. 2020
- [33] S. Sirtkaya, B. Seymen and A. A. Alatan, "Loosely coupled Kalman filtering for fusion of Visual Odometry and inertial navigation," *Proceedings of the 16th International Conference on Information Fusion*, pp. 219-226, Oct.2013.



Rui Sun is currently a Professor in the College of Civil Aviation, Nanjing University of Aeronautics and Astronautics, Nanjing, Jiangsu Province, China. She has a Ph.D. in Intelligent Transport Systems (ITS) from the Imperial College Engineering Geomatics Group (ICEGG) at Imperial College London and holds a M.Sc. in Satellite Positioning Technology from the University of Nottingham. Her research interests include seamless positioning and navigation in challenging environments.



Yeying Dai received a B. S. degree in transportation from Nanjing University of Aeronautics and Astronautics, Nanjing, Jiangsu Province, China in 2021, and is currently a postgraduate student in transportation engineering in Nanjing University of Aeronautics and Astronautics. Her research interest includes multi-sensor integrated navigation for intelligent transportation system applications.



Qi Cheng received Bachelor's and Master's degrees in Transportation Engineering from NUAU, Nanjing, Jiangsu Province, China in 2017 and 2021 and is currently a PhD student in the Department of Land Surveying and Geo-Information at PolyU. His research interest is GNSS NLOS detection algorithms for Intelligent Transport System (ITS) applications.